The Influence of Wettability and Critical Pore–Throat Size Ratio on Snap-off

LI YU (Y. LI)* AND NORMAN CLAUDE WARDLAW†

*Nanhai Western Oil Company, Zhanjiang, People's Republic of China, and †Department of Geology and Geophysics, University of Calgary, Calgary, Alberta T2N 1N4, Canada

Received February 22, 1985; accepted June 25, 1985

Experiments under quasistatic conditions show that the aspect ratio (pore-to-throat effective diameter ratio) necessary for snap-off in throats is ~1.5 when advancing contact angles (θ_A) are equal to zero and increases only slightly, to 1.75, when θ_A is equal to 55°. Above ~70°, snap-off in throats does not occur in systems with pressure equilibrium between pores and throats. Three critical contact angles are recognized for two types of interfaces. Advancing (θ_A) and receding (θ_R) angles for convex interfaces and θ_S, the angle measured for selloidal interfaces at the moment of instability when snap-off occurs. Capillary pressure, disjoining pressure, thin-film thickness, and contact angles are interrelated phenomena and, for a given solid and fluid pair, θ_A, θ_R and θ_S may be defined at different pressures and are not equal but are points on a common curve, the equation for which is defined. As θ_A increases from 0° to 70° we estimate that θ_S increases from 30° to 77°. The difference between θ_S and θ_A decreases with increase in θ_A. The Young–Laplace equation assumes constancy of contact angle and must be applied with caution since contact angle is a function of capillary pressure as well as of interface type.

I. INTRODUCTION

Many natural and artificial porous media consist of larger spaces (pores) connected by smaller spaces (throats) which form continuous three-dimensional networks. During the displacement of nonwetting fluid by wetting fluid (imbibition), collars of wetting fluid may form in throats and these have interfaces with elements of negative as well as positive curvature. That is, radii of curvature occur on both sides of an interface which is selloidal or saddle-shaped (Fig. 1). As capillary pressure is lowered, the curvature of the collar changes to a critical value at which the fluid–fluid interface becomes unstable and suddenly ruptures. Prior to this event, the interface is stable and can be made to advance or retreat in response to small decreases or increases of capillary pressure. Rupturing of a selloidal interface which has become unstable has been referred to as snap-off (1–4) or choke-off (5). It occurs at a critical capillary pressure and curvature which are functions of throat size and wettability. The term snap-off has been applied to events during drainage (1, 2) as well as during imbibition (3, 4).

In addition to selloidal interfaces, interfaces with only positive elements of curvature occur and are referred to as convex interfaces (Fig. 2). Advance or retreat of a convex interface in a pore or throat is referred to as "piston-type" motion (4). For a given wettability, there is a critical pore radius (r_p) to throat radius (r_t) (r_p/r_t = critical aspect ratio) at which snap-off of a selloidal interface occurs in a throat at a higher capillary pressure than a convex interface can advance in the adjacent pore. As a result the nonwetting phase becomes disconnected by snap-off in the throat and nonwetting phase is trapped in the pore. This is an important mechanism of trapping of oil in water-wet reservoir rocks during waterflooding (6). Initially, assume that both pore and throat are simple circular tubes linked in series and, later, we will consider the concept of effective radius for other cross-sectional shapes. If the

0021-9797/86 $3.00

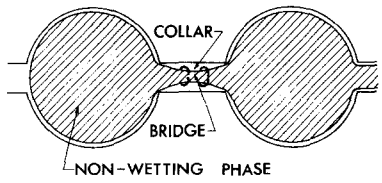

FIG. 1. Two pores with connecting throat to illustrate nonwetting phase bridge (shaded) and wetting phase collar (plain) in throat. Interface is selloidal. The thickness of the continuous wetting film is greatly exaggerated here and also on Figs. 3 and 8.

pore and throat both have circular cross-sectional shape with radii r_p and r_t and the same wettability, the critical aspect ratio is equal to the ratio of the capillary pressure for piston-type advance of a convex interface *in the throat* (P_{pt}) to the capillary pressures for snap-off *in the same throat* (P_{st}). That is, $r_p/r_t = P_{pt}/P_{st}$.

The purpose here is to report the results of experiments which define the critical conditions of aspect ratio and contact angle for snap-off in a single pore–throat pair. Experiments were performed in transparent glass models using several fluid pairs with differing advancing contact angles. Previous workers have reported measurements of critical aspect ratio for snap-off in both imbibition and drainage (2, 7) but these data have been for completely wetted systems (advancing contact angle = 0) and no experimental work is available to relate critical aspect ratio to wettability.

Experiments under quasistatic conditions reported here, for throats of constant rectangular cross section and constant circular cross section, show that the aspect ratio necessary for snap-off in throats is ~1.5 for advancing contact angles (θ_A) equal to zero and increases only slightly to 1.75 for θ_A equal to ~55°. Above 70°, snap-off in throats does not occur in systems with pressure equilibrium between pores and throats. Published experimental data for θ_A equal to zero should be compared to reported critical aspect ratios of ~3.65 (2), ~2.0 (7), and ~2.3 (4), all of which are larger than those determined by us. Existing theoretical treatments fail to explain adequately the relationships established experimentally between critical aspect ratio for snap-off and contact angle.

This paper concerns the conditions for snap-off in a single pore–throat pair. In a subsequent paper (8) we consider the topologic aspects of snap-off in relation to disconnection and entrapment of nonwetting phase in several interconnected pores.

Experiments were performed under quasistatic conditions by decreasing (drainage) and increasing (imbibition) the fluid pressure in the wetting phase (P_w). The nonwetting phase (nwp) is air, in all experiments reported here, and nonwetting phase pressure (P_{nw}) is constant and equal to atmospheric pressure. In a given experiment, advancing contact angles (θ_A) and receding contact angles (θ_R), in imbibition and drainage respectively, are constant but not necessarily equal and represent two limiting conditions for an interface in equilibrium (Fig. 2). Further, the contact angle (θ_S) measured in the wetting phase within a collar (Fig. 2) has a limiting value at the moment of instability where snap-off occurs and this angle is generally not equal to θ_A or to θ_R. Contact angle is measured in the denser phase in the systems reported in this paper. Interfacial tension (γ) is taken to be constant and gravity forces are weak in relation to capillary forces. All fluid motions occur in a horizontal plane.

Entry of nonwetting phase (nwp) into a duct of circular cross section and diameter (d) is achieved at a threshold capillary pressure:

$$P_c = P_{nw} - P_w = \frac{4\gamma \cos \theta_R}{d}. \qquad [1]$$

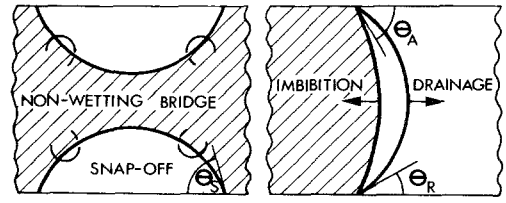

FIG. 2. Selloidal interface (left) and convex interfaces (right) in cylindrical tube with horizontal axis. Two convex interfaces indicate the advancing and retreating positions with contact angle hysteresis ($\theta_A > \theta_R$) (piston-type motion).

Small increases or decreases of this capillary pressure cause the meniscus to advance or recede in a reversible manner (piston-type motions), the difference in capillary pressure being related to contact angle hysteresis.

In a duct of rectangular cross section, of width x and depth y, the threshold capillary pressure for $\theta_R = \theta_A = 0$ is given by Lenormand *et al.* (4) as

$$P_c = F(\epsilon)2\gamma\left(\frac{1}{x} + \frac{1}{y}\right), \quad \text{where } \epsilon = \frac{x}{y} \qquad [2]$$

and

$$F(\epsilon) = \frac{\epsilon(4 - \pi)}{2(1 + \epsilon)\{(1 + \epsilon) - [(1 + \epsilon)^2 - \epsilon(4 - \pi)]^{1/2}\}}. \qquad [3]$$

The dimensionless term $F(\epsilon)$ is nearly equal to 1 and Eq. [2] can be approximated by

$$P_c = 2\gamma\left(\frac{1}{x} + \frac{1}{y}\right)\cos\theta \qquad [4]$$

as given in (9) for any value of θ. The angle θ is not necessarily the same in imbibition as in drainage.

An important difference between smooth ducts of circular cross section and those of rectangular cross section is that the former only have a thin film of wetting fluid separating the nonwetting fluid from the solid over the entire surface whereas, in the latter case, there are larger wedges of wetting fluid associated with the corners of the rectangular plates as well as thin films elsewhere (Fig. 3). One of the conditions for snap-off is that wetting fluid be supplied to specific sites in the throats and the supply rate is affected by these differences in wetting phase distribution. Since sediments and rocks typically have spaces defined by irregular surfaces, a rectangular section provides a more realistic model than a cylindrical tube.

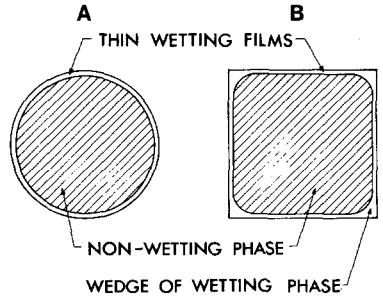

FIG. 3. Conduits of circular and square cross section to illustrate positions of thin films and wedges of wetting phase.

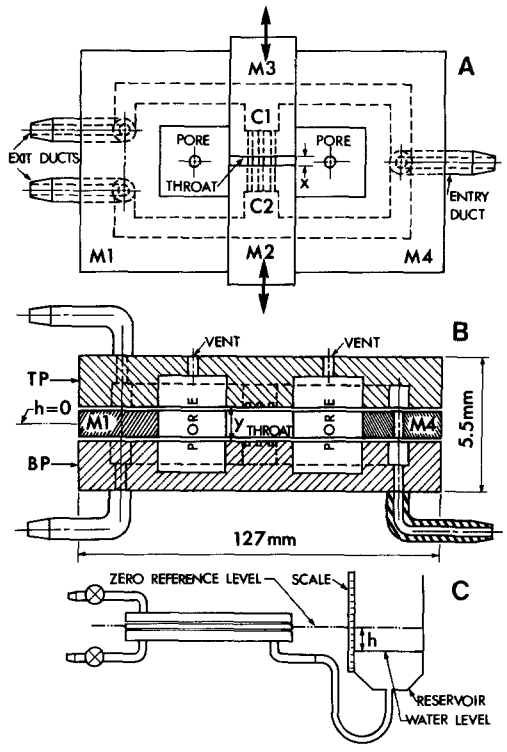

FIG. 4. Experimental apparatus for throat of rectangular cross section.

II. EXPERIMENTS WITH THROATS OF RECTANGULAR CROSS SECTION

A. Experimental Methods

The experimental apparatus is illustrated in plan view and median-longitudinal section in Figs. 4A and B. The throat is of rectangular cross section and fixed depth ($y \cong 1$ mm) but adjustable width ($x \cong 0.5$ mm) so that the effective throat size can be varied.

Wetting fluid can enter the throat along grooves associated with the corners of the rectangular cross section (Fig. 3B) and also

along several grooves etched into the top and bottom plates perpendicular to the long axis of the throat and connecting with local sources of wetting fluid in chambers C1 and C2 (Fig. 4A). The design is such that wetting fluid is always accessible to the throat independently of thin films. This enables rapid attainment of equilibrium when pressure is changed during an experiment. The model consists of three layers: a top plate (TP), a bottom plate (BP), and four middle plates M1 to M4 (Figs. 4A and B). The top and bottom plates both have been etched with HF to provide the ducts illustrated. The middle plates M1 and M4 are "c"-shaped and fixed but the middle plates M2 and M3 can be moved in and out, as indicated by arrows, to change the x dimension of the throat.

One side of the apparatus is connected to a large reservoir of wetting fluid the level of which can be changed by adding or removing liquid with a syringe. The liquid level is read from a fixed scale. The upper plate has two large vents drilled to connect the pores with the atmosphere (Fig. 4A).

Initially, all spaces in the model are filled with wetting liquid by flowing liquid from the reservoir into the entry duct and out of the four exit ducts. The exit ducts are to facilitate clearing the model of trapped air at the beginning of an experiment. Subsequently, valves on the ducts are closed and they have no further part in the experiment.

The starting reference position is with the liquid level in the reservoir at the same elevation as the middle of the middle plate (Fig. 4C). At this stage, menisci of large radius are associated with the two vents which connect the pores to the atmosphere. Liquid is removed slowly from the reservoir with a syringe and, as wetting fluid pressure in the model decreases, the pores fill with air (nonwetting fluid) and menisci enter both ends of the throat from the adjacent pores. At a consistent near-central position in the throat, but before coalescence of the menisci, the elevation of liquid in the reservoir is recorded as a height measured from the reference level (h_{dt} = height for piston-type drainage in throat). By increasing the pressure of the liquid, the menisci withdraw and the height is again measured (h_{pt} = height for piston-type imbibition in throat). Pressure on the liquid is again decreased until the two menisci meet and coalesce. The throat is then air-filled except for thin wetting films and wetting fluid in the grooves and along the corners.

Wetting phase pressure is increased slowly by adding liquid with a syringe until snap-off occurs in the throat. The distance from the reference level (h_{st} = height for snap-off in throat) is recorded. The procedure was repeated over 20 times and average values determined. Since the densities of both fluids are known, as well as the nonwetting phase pressure (atmospheric), the distances h_{dt}, h_{pt}, and h_{st} can be transformed to equivalent capillary pressures which are, respectively, P_{dt}, P_{pt}, and P_{st}.

From Eqs. [1] and [2], an effective diameter (d_e) for a meniscus is obtained

$$d_e = \frac{2}{F(\epsilon)\left(\frac{1}{x} + \frac{1}{y}\right)}. \qquad [5]$$

We were able to verify this relationship for liquid displacing air since the dimensions of the throat (x and y), the surface tension (γ), contact angle ($\theta_R = 0$), and capillary pressure were all independently measured. For fluid pairs with nonzero contact angles, we measured drainage and imbibition capillary pressure and used Eq. [1] with θ_R or θ_A and Eq. [5] to calculate receding and advancing contact angles within the throat. These angles were also calculated independently from capillary rise and fall experiments in cylindrical glass tubes of known bore and determinations by the two methods corresponded closely (Table I). Contact angle hysteresis is small presumably because the glass surfaces are relatively smooth.

Nonzero contact angles were obtained on glass by coating the surface with silicone (Table I). The glass was cleaned in hot sodium hydroxide solution, rinsed thoroughly with dis-

TABLE I

Contact Angles, Fluid Properties, and Capillary Pressures

Fluid pairs and solid	Contact angles: From capillary rise in tube θ_R	Contact angles: From capillary rise in tube θ_A	Contact angles: From measured capillary pressure in model θ_R	Contact angles: From measured capillary pressure in model θ_A	Interfacial (surface) tension, γ (mN/m)	Density of displacing phase, ρ (g/cm^3)	Capillary heads (cm): Drainage, h_{dt}	Capillary heads (cm): Imbibition, h_{pt}	Capillary heads (cm): Snap-off, h_{st}	P_{st}/P_{pt}	Critical aspect ratio, P_{pt}/P_{st}	Effective radii, r_e (cm)
1. Air–water with $KMnO_4$ on clean glass	0	0	0	0	71.7	0.9981	4.45	4.45	3.00	0.67	1.49	0.0331
2. Air-tetradecane on glass coated with silicone	32	34	29	32	25.8	0.7602	1.90	1.85	1.15	0.62	1.61	0.0318
3. Air–pyridine on glass coated with silicone	48	54	52	60	37.4	0.9819	1.48	1.22	0.70	0.57	1.75	0.0321
4. Air–pyridine plus water on glass coated with silicone	62	77	62	73	53.7	0.9891	1.60	1.02	−1.30[a]	−1.27	—	0.0321
5. Air–water on glass coated with silicone	69	87	68	87	71.9	0.9976	1.70	0.20	−2.60[a]	−13.0	—	0.0329
6. Air–water with $KMnO_4$ on clean glass	0	0	0	0	70.4	0.9998	6.70	6.70	4.30	0.64	1.56	0.0215

Note. Systems 1 to 5 were used in the experiments with throats of rectangular cross section and System 6 in a capillary tube of circular section. Surface tensions were measured by the drop-weight technique and capillary rise and densities with a PAAR DMA 45 density meter.

[a] Capillary pressures in the throat for an experiment in which the capillary pressures in throat and pore are not in equilibrium due to restricted supply of wetting phase to the pore.

tilled water and allowed to dry in the air. A siliconizing agent (SurfaSil-Pierce Chemical Co., Ill.) was brushed onto the dry surface with clean tissue for 5 min and then washed-off with distilled water, drained, and allowed to air dry.

B. Results

The ratio of snap-off capillary pressure (P_{st}) to the capillary pressure for piston-type motion of a convex interface in the throat (P_{pt}), is equivalent to the reciprocal of critical aspect ratio. For a single pore–throat pair, any ratio larger than critical means that snap-off occurs in the throat at a higher capillary pressure than nwp can withdraw from the pore. Figure 5 illustrates P_{st}/P_{pt} as a function of advancing contact angle from the data presented in Table I. For $\theta_A = 0$, the critical aspect ratio is ~1.5 and increases to ~1.75 for $\theta_A = 55°$ (Table I). Thus, in the range of contact angles from 0° to 60°, critical aspect ratio is relatively insensitive to contact angle.

Measurements of P_{st}/P_{pt} versus θ_A for angles larger than, as well as somewhat smaller than 70° (8), indicate a unique point at ~70° where the capillary pressure ratio for snap-off changes from positive to negative. Thus, the critical aspect ratio for snap-off appears to become infinite at ~70° and snap-off is not possible

under quasistatic conditions of imbibition (Fig. 6).

The experiments described above for $\theta_A < 70°$ were performed under quasistatic conditions in which wetting phase pressure was constant within the pore–throat region. However, it was observed that snap-off occurred for contact angles greater than 70°, measured in the displacing phase, when wetting phase pressure was increased rapidly such that the wetting phase pressure in the throat was larger than both the nonwetting phase pressure in the throat and the wetting phase pressure in the pore. Unequal wetting phase pressures within the model are possible momentarily because the ducts supplying wetting phase to the throat are larger than those supplying wetting phase to the pore (Fig. 4A). The capillary pressure which is measured is that inside the throat.

III. EXPERIMENTS WITH THROATS OF CIRCULAR CROSS SECTION

A. Experimental Methods

The experimental apparatus consists of a piece of cylindrical capillary tubing of 0.215 mm internal radius which is open at both ends and breached by a fine saw-cut which connects the capillary bore to a surrounding sleeve (Fig. 7). The saw-cut extends over about one-tenth of the circumference of the tube. The sleeve is connected to a reservoir as depicted in Fig. 4C and the experiment is conducted much as in the case of the rectangular throat model.

The tube and sleeve are saturated with wetting liquid and the zero reference scale in the reservoir is leveled with the center of the capillary bore. Pressure is lowered by removing water from the reservoir with a syringe and air (nonwetting phase) enters both ends of the capillary tube. The distance between the reservoir water level and the zero mark is recorded during drainage (h_{dt}). Similar measurements are made for imbibition (h_{pt}) by adding water to the reservoir until the level is such that interfaces begin to withdraw from the tube. The wetting phase pressure is again lowered until the interfaces are allowed to coalesce at the saw mark. The system is allowed

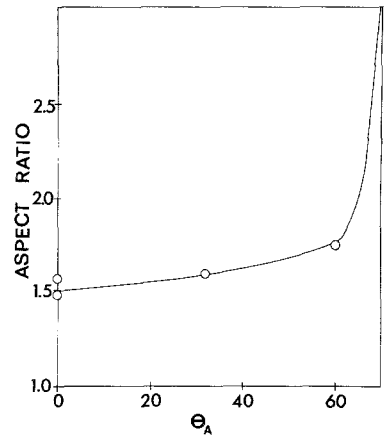

FIG. 6. Data from Fig. 5 expressed in terms of aspect ratio (pore-to-throat effective diameter ratio).

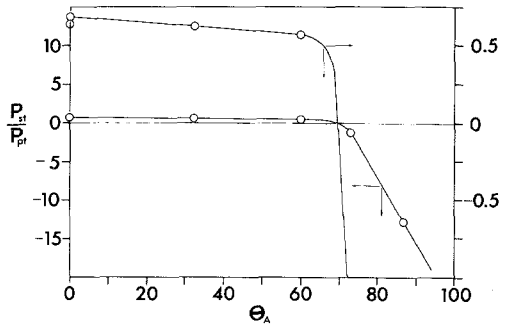

FIG. 5. Ratio of snap-off capillary pressure in a throat (P_{st}) to capillary pressure for advance of convex interface in the same throat (P_{pt}) as a function of advancing contact angle. The right- and left-hand axes are both P_{st}/P_{pt} shown at different scales. Experimental data for systems summarized in Table I.

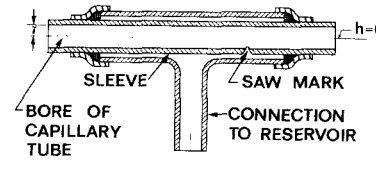

FIG. 7. Experimental apparatus for throat of circular cross section.

to equilibrate and the wetting phase pressure is increased until a wetting phase collar adjacent to the saw cut becomes unstable and snap-off occurs. The water level is recorded (h_{st}) and the experiment can be repeated after draining wetting fluid from the tube and allowing time for equilibration. The distances h_{dt}, h_{pt}, and h_{st} can be converted to capillary pressure P_{dt}, P_{pt}, and P_{st}, as previously, and these are recorded in Table I. The equivalent reciprocal critical aspect ratios (P_{st}/P_{pt}) and critical aspect ratios are shown in Figs. 5 and 6, respectively.

B. Results

For $\theta_A = 0$, P_{st}/P_{pt} equals 0.64 and the reciprocal gives the equivalent critical aspect ratio of 1.56. The corresponding value for the throat of rectangular cross section was 1.49. Thus, these cross-sectional shapes do not have much effect on snap-off capillary pressure under quasistatic conditions of displacement.

IV. DISCUSSION

Fluid interfaces are either convex or selloidal (saddle-shaped) (Fig. 2). For the former, the two principal radii of curvature are on the same side of the interface and for the latter on opposite sides. Interfaces during snap-off are selloidal and, in some respects, resemble liquid bridges. Plateau (10) showed that all stable liquid bridges are surfaces of constant mean curvature but that not all surfaces of constant mean curvature are stable. For example, a cylinder of length-to-diameter ratio greater than the constant pi, between fixed circular end plates, will break up (10, 11).

However, in a tube with thin liquid films separating a nonwetting fluid from the solid walls, a fluid cylinder can be stable at length-to-diameter ratios greater than pi. Molecular interactions in the thin films, referred to as disjoining pressures (π), serve to stabilize the interface. Stable fluid interfaces have constant mean curvature except within the thin film region where disjoining pressures are large (7, 12–14). The force-balance across a static interface between two fluids is described by the Laplace equation

$$P_{nw} - P_w = P_c = 2H\gamma, \qquad [6]$$

where $2H$ is the curvature of the fluid–fluid interface. Equation [6] for cylindrical symmetry is

$$P_c = \frac{\gamma}{r}\, d(r/\sqrt{1 + (dr/dz)^2})/dr, \qquad [7]$$

where r is the interface radius and z is distance measured along tube axis from the interface (Fig. 8A).

For the boundary conditions

$$r = R,\ dr/dz = \tan\theta, \quad \text{at} \quad z = A$$

$$r = 0,\ dr/dz = \infty, \quad \text{at} \quad z = 0,$$

where R is the radius of the tube and θ the contact angle. Integration of Eq. [7] for the given boundary conditions yields

$$\frac{RP_c}{2\gamma} = \cos\theta \qquad [8]$$

which is the Young–Laplace equation.

The contact angle θ here is the angle between the solid surface and a tangent line from

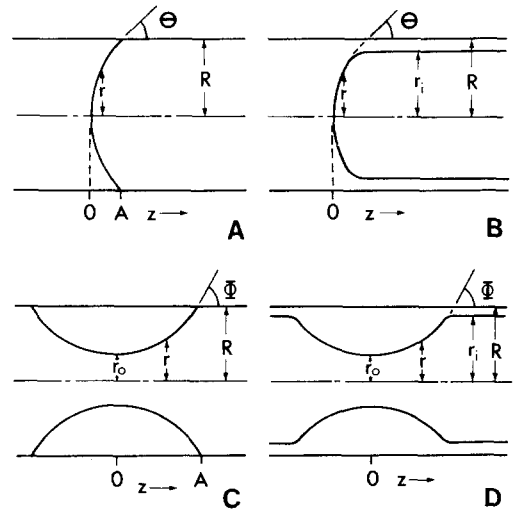

FIG. 8. Convex interfaces: (A) with a contact angle; (B) with thin film. Selloidal interfaces: (C) with a contact angle; (D) with thin film.

the region of constant interface curvature undistorted by the local disjoining pressure. The effects of the disjoining pressure are recognized in the augmented Young–Laplace equation (Eq. [9]) which is valid uniformly from thin-film to bulk layer,

$$P_c = 2H\gamma + \pi(h). \quad [9]$$

Here $\pi(h)$ is the disjoining pressure which varies with thin film thickness (h). The additivity of disjoining pressure in Eq. [9] is a hypothesis introduced by Derjaguin (12) and reviewed in detail by Mohanty *et al.* (13). It emphasizes that the pressure drops and curvatures across the thin film and across the interface between bulk liquids are not the same. As pointed out by Melrose (14), the net repulsive force in a stable thin film (equivalent to disjoining pressure $\pi(h)$) is equivalent to the difference between the capillary pressures across an interface for bulk fluids and a thin film interface.

For cylindrical symmetry Eq. [9] is written

$$P_c = \left(\frac{\gamma}{r}\, d(r/\sqrt{1 + (dr/dz)^2})/dr\right) + \pi(R - r), \quad [10]$$

where $\pi(R - r)$ is the disjoining pressure for a film thickness (h) which is equivalent to ($R - r$) (Fig. 8B).

For the boundary conditions

$$r = r_i,\ dr/dz = 0, \quad \text{at} \quad z = \infty$$

$$r = 0,\ dr/dz = \infty, \quad \text{at} \quad z = 0.$$

Integration of Eq. [10] for the given boundary conditions gives

$$\frac{RP_c}{2\gamma} = 1 + \frac{1}{R\gamma}\int_0^{r_i} r\pi(R - r)dr. \quad [11]$$

The ratio $P_c/2\gamma$ is a curvature and we shall refer to

$$\frac{P_c}{2\gamma}\Big/\frac{1}{R} = \frac{RP_c}{2\gamma}$$

as a normalized curvature.

From Eqs. [8] and [11] we derive a relation between contact angle and disjoining pressure,

$$\cos\theta = 1 + \frac{1}{R\gamma}\int_0^{r_i} r\pi(R - r)dr, \quad [12]$$

where θ is the contact angle. This shows that contact angle is a function of disjoining pressure and film thickness. Since film thickness is a function of P_c, it follows that contact angle is a function of P_c.

The thickness of thin films is much exaggerated in Figs. 1, 3, and 8. No measurements of thin film thickness were made in this study but such films can be thought of as in the range $\sim 10^2$ to 10^4 Å and for a review of data on the dependence of disjoining pressure on film thickness the reader is referred to Mohanty (7).

We were able to observe that apparent contact angle (Φ) for a selloidal interface increased and bridge length increased (distance from bridge center to contact point A, Fig. 8C) as capillary pressure decreased but were unable to make accurate measurements of Φ in the apparatus used. Corrections from apparent to true contact angles for convex fluid interfaces can be made easily in cylindrical tubes but this is not the case for selloidal interfaces whose surface shape is complex and not known. We do not know of published experimental measurements of contact angles within selloidal bridges as a function of capillary pressure.

In the case of contact angle hysteresis ($\theta_A \neq \theta_R$), an interface in a capillary tube of uniform radius can be in equilibrium over a range of pressures and the two angles define the limits of equilibrium of the interface (Fig. 2). The simple form of the Young–Laplace equation is insufficient to explain the relationships of pressure and interface curvature within this range of pressures.

We will now show that at snap-off, the liquid-fluid angles at the three-phase line where a selloidal interface (elements of positive and negative curvature) contacts solid are larger than contact angles for convex interfaces (elements of positive curvature only).

With the following boundary and symmetry conditions

$$r = R,\ dr/dz = \tan \Phi, \quad \text{at} \quad z = A$$

$$r = r_0,\ dr/dz = 0, \quad \text{at} \quad z = 0,$$

where r_0 is the radius of the bridge at its narrowest point and Φ is the angle of a tangent line from the constant curvature interface, at the contact line, to the wall of the tube (Fig. 8C). The point A, seen in section (Fig. 8C), is the apparent contact point where the fluid interface intersects the cylinder walls.

Applying these boundary conditions and integrating Eq. [7] yields

$$\frac{P_c R}{2\gamma}\left[1 - \left(\frac{r_0}{R}\right)^2\right] + \frac{r_0}{R} = \cos \Phi. \quad [13]$$

If we integrate Eq. [10], the augmented Young–Laplace equation, for the boundary conditions (Fig. 8D)

$$r = r_i,\ dr/dz = 0, \quad \text{at} \quad z = \infty$$

$$r = r_0,\ dr/dz = 0, \quad \text{at} \quad z = 0$$

we get, for a selloidal interface:

$$\frac{P_c R}{2\gamma}\left[1 - \left(\frac{r_0}{R}\right)^2\right] + \frac{r_0}{R} = 1 + \frac{1}{R\gamma}\int_{r_0}^{r_i} r\pi(R - r)dr. \quad [14]$$

Equations [13] and [14] give the relationship between Φ and the disjoining pressure, for the case of a liquid bridge in equilibrium in a cylindrical tube, as

$$\cos \Phi = 1 + \frac{1}{R\gamma}\int_{r_0}^{r_i} r\pi(R - r)dr. \quad [15]$$

Equation [12] gives the relationship between contact angle and disjoining pressure for a convex interface and Eq. [15] provides the equivalent relationship for a selloidal interface. Since disjoining pressure $\pi(R - r)$ is a sensitive function of film thickness $(R - r)$, i.e., Mohanty (7) cites disjoining pressure proportional to $1/(R - r)^n$ where n is of order 3, the contribution to the integral of the lower limit in Eq. [12] is negligible except in the case of very small tube diameters. Since disjoining pressure decreases abruptly as thin-film thickness increases, the contribution to the integral at the lower limit in Eq. [15] is also negligible except for the case where the liquid-fluid interface is cylindrical and remains within the thin-film region where disjoining pressure is relatively large. Equations [12] and [15] become identical in those cases where the contribution to integrals from the lower boundary conditions are zero. Thus, except for the cases where throats or pores are extremely small or where the bridge form is close to being a cylinder, the contact angles for both convex and selloidal interfaces (Fig. 2) in a cylindrical tube of constant bore are given, to a good approximation, by Eq. [12]. In view of this we take the three critical contact angles (θ_A, θ_R, θ_S) as lying on a common curve, given by Eq. [12]. Normally they will not be of the same value!

Equations [8], [11], [13], and [14] are force-balance equations. An interface will be in equilibrium if both sides of the equations are equal. However, not all interfaces which satisfy the force-balance equation are stable. Stability requires that the potential energy be a local minimum with respect to all admissible shape fluctuations. The admissible fluctuations are those which satisfy the constraints on volume and the boundary conditions. If the second variation in energy is negative for any admissible perturbation, then the interface is unstable (7).

Energy is a function of surface area (S) at constant volume (V). In order to obtain V and S we must first find the equation of the interface implied by Eq. [7]. For the boundary condition, $r = R$, $dr/dz = \tan \theta$, at $z = A$ (Fig. 8C), we have

$$dr/dz = \left[4(r/R)^2 \Big/ \left\{2\cos\theta + (P_c R/\gamma)\left[\left(\frac{r}{R}\right)^2 - 1\right]\right\}^2 - 1.\right]^{1/2} \quad [16]$$

Integration of Eq. [16], for a chosen P_c, R, γ, to $r = R$, $z = A$ (where $(dr/dz)_{z=A} = \tan \theta$) gives the profile $r = f(z)$ for the surface. The profiles of the interfaces are then known and can be used to calculate V and S.

Erle *et al.* (11) have in fact calculated V and S for essentially the same problem, the stability for liquid bridges between spheres. Their equation for the profile of the bridge (Eq. [11] of Ref. (11)) is readily seen to be identical to our Eq. [16] on setting: $\psi = 90 - \theta$, $R_s = R/\sin\psi = R/\cos\theta$, $J = -P_c/\gamma$, $Y_c = \cos\theta$, $\dot{Y} = -dr/dz$. R_s is the sphere radius in Erle *et al.* (11). They provided a map of bridge solutions with ψ as ordinate and the mean, i.e., normalized, curvature of the bridge as abscissa. Erle *et al.* used subsets of solutions whose elements all have the same volume and other subsets whose elements all have the same separation to locate solutions for selected volumes and selected separations and found that there could be two solutions, one solution or no solutions, depending on the particular selection of volume and separation. They considered the separations of bridges along a curve of constant volume and found that there was one solution on this curve which has greater separation than any other solution. They called this solution of maximum separation, located at the point of tangency of the constant volume curve with the curve of constant separation, X_{max}. By considering all constant volume and constant separation curves they defined a "locus of tangency" which, they conjectured, marks the boundary between a stable field and an unstable field on the map. Points falling on this locus represent conditions which give single solutions of Eq. [11] of Erle *et al.* or our Eq. [16]. Their conjecture was substantiated by their experimental results. In Fig. 9 we present the result of Erle *et al.* (cf. Ref. (11), Fig. 4) when applied to a bridge within a cylindrical tube and for our notation. The solid line in Fig. 9 is the locus θ_S and is the boundary between stable (upper) and unstable (lower) domains.

We have measured the snap-off capillary pressure P_{st} for several fluid pairs and wettabilities in the tubes of uniform cross section, Table I and Figs. 5 and 6. With these measurements and the results of Erle *et al.*, as given in Fig. (9), we can obtain the relation between θ_A and the contact angle θ_S at snap-off. That

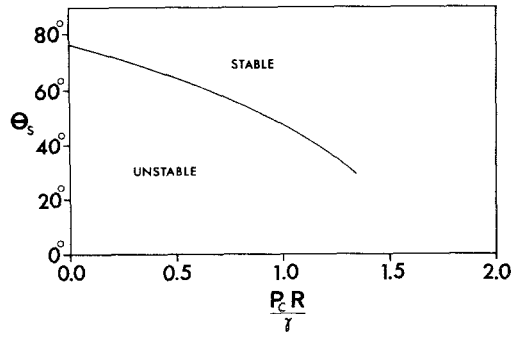

FIG. 9. Critical contact angle at snap-off (θ_S) as a function of normalized capillary pressure for bridges within a cylindrical tube is derived from Erle *et al.* (11) for liquid bridges between spheres.

is, in Table I we give θ_A and P_{st} for each fluid pair and from Fig. 9 we can obtain θ_S corresponding to this same value of capillary pressure (P_{st}). These values of θ_S and θ_A for corresponding fluid pairs are plotted in Fig. 10 (the upper curve and the left-hand ordinate). Now (see Sect. II and Table I) we have also experimentally determined corresponding θ_A and θ_R values (these are given in the lower curve and right-hand ordinate in Fig. 10). Using this relation between θ_A and θ_R and the relation between P_{st} and θ_A we can obtain the relation between P_{st} and θ_R. As a result, we now have all three corresponding pairs θ_R and P_{dt}, θ_A and P_{pt}, and θ_S and P_{st}. For a given wettability, the three angles and pressures will fall on a common curve given by Eqs. [12] and [15]. In Fig. 11 we have displayed these three pairs for three fluid pairs with different wettabilities. The broken line going through θ_S, θ_A, and θ_R for a given fluid pair is taken to represent the functional relation between θ and P_c already given in Eq. [12] or its extension Eq. [15]. The basis for this assertion is that Eqs. [12] and [15] connect capillary pressures and angles which are in balance. Indeed, the points on Fig. 11 are not only in balance but also represent a stable balance.

The capillary pressures at which a convex interface advances and retreats in a tube of constant bore commonly are observed to be different (hysteresis) and different from the

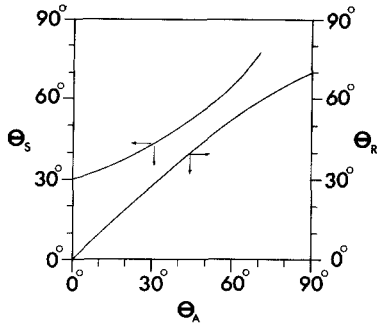

FIG. 10. Critical advancing (θ_A) and receding (θ_R) contact angles determined experimentally for smooth glass of apparatus. The relation between θ_S and θ_A for bridges within a cylindrical tube is derived by transformation of the result of Erle *et al.* (11) for liquid bridges between spheres and applying experimentally measured capillary pressures at snap-off.

capillary pressure of snap-off for the same fluids in the same tube (Table I). Mohanty *et al.* (5, 7, 13) assumed that contact angle is constant for a given system and that the contact angle for a selloidal interface was the same as for a convex interface. This led to the result that as a nonwetting phase bridge narrows (Fig. 2) capillary pressure increases which is the reverse of what is observed experimentally. It is unfortunate that applications of the Young–Laplace equation (Eq. [1]) frequently assume that contact angle is constant for specified fluids and solids and is independent of capillary pressure or interface type. In fact, both capillary pressure and interface type (convex or selloidal) can affect contact angles.

The extension of our results to other situations should be undertaken only with care for both the geometry of the boundaries (e.g., a diverging tube) and the nature of the boundaries of the bridge (wetting or nonwetting) will affect the analysis. Critical aspect ratio for snap-off in throats of circular or rectangular cross section may be a function of throat length. Our experimental results are limiting values for "long throats" whose cross sections are uniform and whose length is two or more times greater than the effective diameter (d_e). This is the common condition in consolidated porous media such as reservoir rocks where the prevailing geometry of throats is sheet-like. However, another common throat type is that typical of unconsolidated media where, say, particles are of approximately spherical form. If throat size is defined as the dimension of minimum area of cross section between adjacent particles, throats are effectively very short and the contact points of selloidal fluid interfaces with the spherical solid surfaces may lie away from such minimum cross sections. Critical aspect ratio for throats of this type will be larger than for those reported here for long throats.

Further, although our analysis has attempted to incorporate a disjoining pressure we have not included the potential role of surface roughness (14–16).

V. CONCLUSIONS

Experiments under quasistatic conditions reported here, for throats of constant rectangular cross section and constant circular cross section, show that the aspect ratio (pore-to-throat effective diameter ratio) necessary for snap-off in throats is ~1.5 for advancing contact angles (θ_A) equal to zero and increases only slightly to 1.75 for θ_A equal to 55°. Above ~70°, snap-off in throats does not occur in systems with pressure equilibrium between pores and throats.

Three critical contact angles are recognized for two types of interface: advancing (θ_A) and receding (θ_R) angles for convex interfaces and

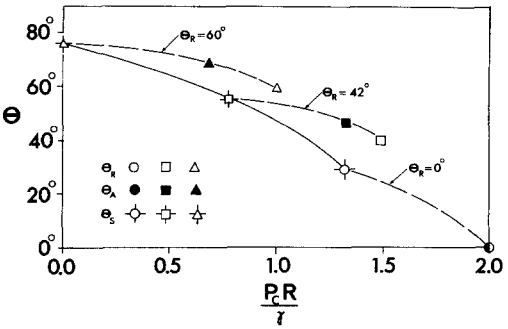

FIG. 11. Critical contact angles (θ_A, θ_R, θ_S) given as a function of normalized capillary pressure based on information from Figs. 5, 6, 9, and 10 and Eqs. [12] and [15]. The solid line is the same curve as on Fig. 9.

angles measured for selloidal interfaces at the moment of instability when snap-off occurs (θ_S). Capillary pressure, disjoining pressure, thin-film thickness and contact angles are interrelated phenomena and, for a given fluid pair and solid, θ_A, θ_R, and θ_S may be defined at different capillary pressures and are not equal but are points falling on a common curve defined by Eq. [12]. As θ_A increases from 0° to 70° we estimate that θ_S increases from 30° to 77°. The difference between θ_S and θ_A decreases with increase in θ_A. Hence the widely used Young–Laplace equation with a constant contact angle must be applied with caution since contact angle is clearly a function of capillary pressure as well as of interface type.

For convex interfaces, where radii of curvature all lie on the same side of the interface, the constraints of the Laplace equation on shape are much more severe than for selloidal interfaces where radii of curvature lie on opposite sides of the interface and a much wider range of stable curvatures are possible. Capillary pressure is related to curvature and disjoining pressure to capillary pressure. Both θ and Φ are related to disjoining pressure. Therefore, the wide range of stable selloidal shapes manifests itself in a wide range of possible values of Φ for stable bridges. This is contrary to previous treatments where it was assumed that Φ is equal to θ.

A duct of uniform rectangular cross section can be assigned an effective diameter (d_e) using Eq. [5] and, with respect to θ_A, θ_R, and θ_S, the behavior is the same as that of a uniform tube of circular section and diameter d_e. Thus, the results can be applied to throats or pores of uniform cross section but differing shape.

This paper has concerned the conditions for snap-off in a single pore–throat pair. In a subsequent paper (8) we consider the topologic aspects of snap-off in relation to disconnection and entrapment of nonwetting phase in several interconnected pores. This work provides the basis for computer modeling of 2-phase fluid displacement processes in porous media of specified geometry and topology.

ACKNOWLEDGMENTS

Financial assistance from the Government of the People's Republic of China and a grant-in-aid of research from the Natural Sciences and Engineering Research Council of Canada are gratefully acknowledged. Dr. W. G. Laidlaw, Dept. of Chemistry, University of Calgary, critically read the manuscript and suggested several important improvements. Mr. W. Tang Kong assisted with preparation of illustrations and Ms. M. Boody typed the manuscript. We thank all of them for their various contributions.

REFERENCES

1. Pickell, J. J., Swanson, B. F., and Hickman, W. B., *Soc. Pet. Eng. J.*, **6,** 55 (1966).
2. Roof, J. G., *Soc. Pet. Eng. J.*, **10,** 85 (1970).
3. Chatzis, I., Morrow, N. R., and Lim, H. T., *Soc. Pet. Eng. J.* **23,** 311 (1983).
4. Lenormand, R., Zarcone, C., and Sarr, A., *J. Fluid Mech.* **135,** 337 (1983).
5. Mohanty, K. K., Davis, H. T., and Scriven, L. E., Soc. Pet. Eng., 55th Ann. Conf., Dallas, SPE 9406 (1980).
6. Stegemeier, G. L., *in* "Improved Oil Recovery by Surfactant and Polymer Flooding" (D. O. Shah and R. S. Schechter, Eds.), p. 55. Academic Press, New York, 1977.
7. Mohanty, K. K., "Fluids in Porous Media: Two Phase Distribution and Flow," PhD thesis. Univ. of Minnesota (1981).
8. Li, Y., and Wardlaw, N. C., *J. Colloid Interface Sci.* **109,** 473 (1986).
9. Lenormand, R., and Zarcone, C., Soc. Pet. Eng., 59th Ann. Conf., SPE 13264 (1984).
10. Plateau, J. A. F., "Experimental and Theoretical Researches on the Figures of Equilibrium of a Liquid Mass," translation in Ann. Rept. Smithsonian Institution (1863–1866).
11. Erle, M. A., Dyson, D. C., and Morrow, N. R., *AIChE J.* **17,** 115 (1971).
12. Derjaguin, B. V., *in* "Proceedings, 2nd International Congress on Surface Activity," Vol. 2, p. 153. 1957.
13. Mohanty, K. K., Davis, H. T., and Scriven, L. E., *in* "Surface Phenomena in Enhanced Oil Recovery" (D. O. Shah, Ed.), p. 595. Plenum, New York, 1981.
14. Melrose, J. C., Soc. Pet. Eng., 57th Ann. Conf., New Orleans, SPE 10971 (1982).
15. Morrow, N. R., and McCaffery, F. G., *in* "Wetting Spreading and Adhesion" (J. F. Padday, Ed.), p. 289. Academic Press, New York, 1978.
16. Joanny, J. F., and de Gennes, P. G., *J. Chem. Phys.* **83,** 552 (1984).